Available online at www.sciencedirect.com
SCIENCE DIRECT®
Journal of Magnetic Resonance 165 (2003) 153–161
JMR Journal of Magnetic Resonance
www.elsevier.com/locate/jmr

Effects of finite-width pulses in the pulsed-field gradient measurement of the diffusion coefficient in connected porous media

Lukasz J. Zielinski[a,b,*] and Pabitra N. Sen[a]

[a] *Schlumberger-Doll Research, 36 Old Quarry Road, Ridgefield, CT 06877-4108, USA*
[b] *Department of Physics, Harvard University, Cambridge, MA 02138, USA*

Received 22 June 2003; revised 26 June 2003

Abstract

We analytically compute the apparent diffusion coefficient D_{app} for an open restricted geometry, such as an extended porous medium, for the case of a pulsed-field gradient (PFG) experiment with finite-width pulses. In the short- and long-time limits, we give explicit, model-independent expressions that correct for the finite duration of the pulses and can be used to extract the pore surface-to-volume (S/V) ratio as well as the tortuosity. For all times, we compute D_{app} using a well-established model form of the actual time-dependent diffusion coefficient $D(t)$ that can be obtained from an ideal narrow-pulse PFG. We compare D_{app} and $D(t)$ and find that, regardless of pulse widths and geometry-dependent parameters, the two quantities deviate by less than 20%. These results are in sharp contrast with the studies on closed geometries [J. Magn. Reson. A 117 (1995) 209], where the effects of finite gradient-pulse widths are large. The analytical results presented here can be easily adapted for different pulse protocols and time sequences.

Keywords: Restricted diffusion; Porous media; Pulsed-field gradient stimulated echo; Narrow-pulse approximation; Surface-to-volume ratio

1. Introduction

Pulsed-field gradient (PFG) techniques have become an indispensable part of imaging and diffusion measurements using nuclear magnetic resonance (NMR) [1–4]. Under the narrow-pulse approximation, i.e., when diffusion during the encoding and decoding gradient pulses can be ignored, the measured signal gives the Fourier transform of the conditional probability distribution of displacements between the pulses. Geometrical restriction is encoded in the dynamics and reflected in the magnitude of the formed echo [5–9]. A quantity commonly extracted from a PFG measurement that is of great usefulness for probing the structure of the confining geometry is the time-dependent diffusion coefficient $D(t)$. In three dimensions, it is related to the mean-square displacement of the spin-bearing molecules by

$$D(t) \equiv \frac{\langle [\mathbf{x}(t) - \mathbf{x}(0)]^2 \rangle}{6t}. \tag{1}$$

In the case of an ideal pulsed-field gradient stimulated echo (PFGSTE) experiment, with narrow gradient pulses of duration δ and magnitude g, spaced by a diffusion time Δ (see Fig. 3), $D(t)$ is obtained from the initial slope of the attenuation exponent with respect to $k^2 \equiv \gamma^2 g^2 \delta^2$,

$$D(\Delta) = -\frac{1}{\Delta} \lim_{k \to 0} \frac{\partial}{\partial (k^2)} \ln \left(\frac{M(t_E)}{M_0} \right), \tag{2}$$

where γ is the gyromagnetic ratio and t_E the echo formation time. When the narrow-pulse approximation breaks down, however, this procedure for computing $D(t)$ is no longer valid.

There have been a number of studies trying to understand the effects of this breakdown [8–14] as it frequently cannot be avoided. First, noble gases, such as xenon, are finding increasing use as a probe of porous media. Since the mobility of gas molecules is high, the effects of restricted diffusion during the encoding and decoding periods cannot be ignored [9]. Second, in many medical and petrophysical applications, the gradients

* Corresponding author. Fax: 1-2034383819.
E-mail address: lzielinski@ridgefield.oilfield.slb.com (L.J. Zielinski).

1090-7807/$ - see front matter © 2003 Elsevier Inc. All rights reserved.
doi:10.1016/S1090-7807(03)00248-9

used are weak, either due to hardware constraints or, as in experiments involving living tissue, by design [15,16]. Consequently, they must be applied for longer periods of time during which diffusion may be substantial. Finally, pulse sequences used to cancel the effects of internal fields in media with strong susceptibility contrasts, tend to be long [17–20], again enhancing the effects of diffusion.

Previous studies of the breakdown of the narrow-pulse approximation have been limited to the short-time regime [8] and to isolated pores [10–13], though the center-of-mass-propagator picture of Mitra and Halperin [14] offers some qualitative general insights. The primary focus of the present paper is diffusion in a homogeneous open geometry, such as a connected porous medium with a well-defined long-time effective diffusion coefficient. We draw a schematic picture of what we mean by "open" and "closed" geometries in Fig. 1. Part (a) is a closed geometry, such as an isolated pore or cell; Part (b) is a highly constricted open geometry; and Part (c) is a dilute suspension, an open geometry where restriction is a small perturbation. We provide analytical results that cover all the parameter space. Using the Gaussian phase or second cumulant approximation (GPA) framework developed in [21], we compute the attenuation exponent of the magnetization at echo time t_E, which is given by the mean-square average of the phases accumulated by the diffusing spins, $\langle\varphi^2(t_E)\rangle/2$. The GPA in closed geometries has been studied extensively and shown to have a broad range of validity [10,22–25]. Since the regimes of its validity in open geometries are not well established, we discuss them in some detail in Appendix A and sketch them in Fig. 7 in the $\delta - \Delta$ parameter space.

Before giving the details of the calculation, it is worthwhile to contrast the gross features of the attenuation in closed and open geometries. In Fig. 2, we plot the computed attenuation exponent for the PFGSTE as a function of the diffusion length for unbounded space (long dashes), for a one-dimensional closed pore of size L_S (short dashes), and for an open geometry (solid line) with size fixed by its surface-to-volume (S/V) ratio via

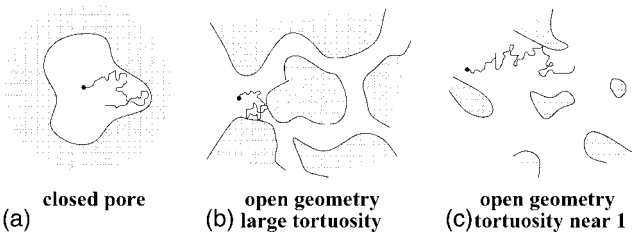

Fig. 1. Three possible types of geometries: (a) closed geometry such as an isolated pore or cell; (b) open geometry with large amount of restriction (tortuosity $\mathcal{T} \gg 1$); and (c) open geometry with small amount of restriction ($\mathcal{T} \approx 1$). Unbounded space is an open geometry with tortuosity $\mathcal{T} = 1$.

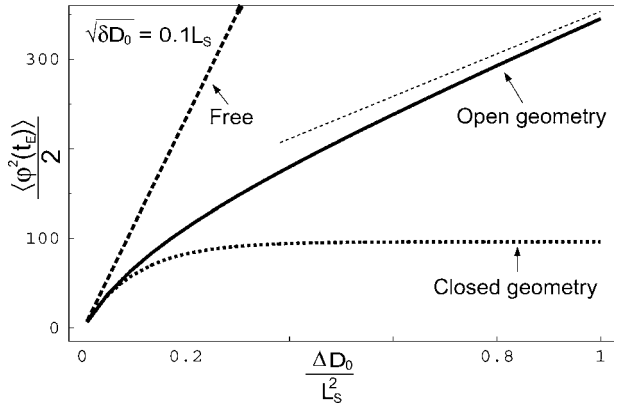

Fig. 2. GPA (Gaussian phase approximation) attenuation exponent, in units of $8\pi^{-8}L_S^2\gamma^2g^2\delta^2$, for the narrow-pulse PFGSTE (pulsed-field gradient stimulated echo) as a function of the diffusion time Δ between the encoding and decoding gradients. Here g is the gradient magnitude, δ the pulse width, and γ the gyromagnetic ratio. L_S is the characteristic length of the system, determined by the size of the one-dimensional box for the closed geometry and by the surface-to-volume (S/V) ratio for the open geometry, $L_S = (9\sqrt{\pi}/4)(V/S)$. The closed-geometry curve is the same as in [10, Fig. 2], and the open-geometry curve is computed using the formalism of Section 2 as applied to the PFGSTE in Section 3.

$(9\sqrt{\pi}/4)(V/S) = L_S$. The encoding and decoding periods of duration δ are taken short, $\sqrt{\delta D_0} = 0.1L_S$, so that the curves are close to the ideal narrow-pulse limit. The fundamental difference between a connected open geometry and a closed pore is that at long diffusion times the attenuation exponent grows linearly with time for open geometries (asymptotic thin dotted line) but saturates to a time-independent constant for closed geometries.

At short times the diffusion process is insensitive to the macroscopic morphology of the system and thus cannot distinguish between closed and open geometries. The short-time diffusion coefficient depends only on the total pore surface-to-volume (S/V) ratio [5],

$$D(t)|_{\text{short}} = D_0\left[1 - \frac{4}{9\sqrt{\pi}}\frac{S\sqrt{D_0 t}}{V}\right]. \tag{3}$$

Differentiation appears at longer times, when the spins have had sufficient time to traverse distances of the order of the structural length scales present.

In closed geometries, the mean-square displacement saturates and the attenuation of the magnetization plateaus. $D(t)$ goes to zero inversely with time with higher-order terms decaying exponentially. In a one-dimensional pore of size L_S, for example,

$$D(t)|_{\text{closed}} \overset{t\to\infty}{\to} \frac{L_S^2}{12t}. \tag{4}$$

In the limit of both long δ and long Δ, this corresponds to Neuman's result [10,22], which is independent of Δ:

$$-\ln\frac{M(t_E)}{M(0)}\bigg|_{\text{closed}} = \frac{\langle\varphi^2(t_E)\rangle}{2} = \frac{g^2\gamma^2L_S^4\delta}{60D_0}. \tag{5}$$

In open geometries, on the other hand, for long times the diffusion coefficient reaches a time-independent asymptotic form known as the "tortuosity limit,"

$$D(t)|_{\text{open}} \overset{t\to\infty}{\to} \frac{D_0}{\mathcal{T}} \equiv D_\infty. \tag{6}$$

It is reduced from the unbounded value of D_0 by a geometrical factor $\mathcal{T}$, called the tortuosity, that characterizes the medium. In fact, on general grounds it has been argued [26] that the long-time expansion of $D(t)$ in an open geometry should take the model-independent form,

$$D(t)|_{\text{open}} \overset{t\to\infty}{\to} D_\infty + \frac{\kappa_1}{t} + \frac{\kappa_2}{t^{3/2}} + \cdots, \tag{7}$$

where the constants κ_1 and κ_2 depend on the details of the geometry. This expansion implies that, for long times, the mean-square displacement of the diffusing spins, and consequently the attenuation exponent, will grow linearly with time.

Extracting the time-dependent diffusion coefficient from the measured attenuation exponent becomes complicated when pulses cannot be assumed narrow and Eq. (2) is inapplicable. The quantity one can obtain, however, is an *apparent* diffusion coefficient, D_{app}, extracted from the measured signal with the use of free-diffusion formulas for the particular pulse sequence [27]. We will find that for open geometries, D_{app} converges to the actual $D(t)$ both in the long- and short-time limits, and quite generally, does not deviate much from it throughout the entire range of t. This is consistent with the results of Tanner [27], who studied diffusion in a one-dimensional periodic system with identical permeable barriers and found $D_{\text{app}} \approx D(t)$ for weak gradients (where the GPA is valid). In this paper, we study a more general porous medium and show how geometric quantities of interest, such as the surface-to-volume ratio and the tortuosity of the bounding space, can be obtained from D_{app} directly, even in the presence of finite-width pulses when the measurement of $D(t)$ may not be possible.

2. General expressions for spatially uniform gradients

We consider a system of spins diffusing in a restricted isotropic geometry with zero surface relaxivity in a time-dependent applied gradient $g(t)$. The more general case of an arbitrary inhomogeneous magnetic field is considered in [21]. We further assume that $g(t)$ is piecewise constant in time, as in a variety of pulsed-NMR experiments, and suppress bulk relaxation. A general pulse shape, however, can be accommodated by Eqs. (9) and (10). To take into account the radiofrequency (RF) pulses, we follow the standard procedure [4] and introduce an *effective* gradient $g(t)q(t)$ that determines the amount of phase acquired by the spins in a given pulse sequence. $q(t)$ is the appropriate coherence pathway [28], with $q(t) = 0$ when the magnetization is aligned along the z-axis or $q(t) = \pm 1$ when in the transverse plane. A complete exposition of the coherence pathway formalism in the form used in this paper can be found in [21] or [29]. In Section 3, we write down the values of $q(t)$ for the PFGSTE.

The total phase will be zero at the echo time t_{E},

$$\int_0^{t_{\text{E}}} g(t)q(t)\,\mathrm{d}t = 0, \quad q(t) = 0, \pm 1. \tag{8}$$

The total magnetization, then, within the GPA, is given by

$$M(t_{\text{E}}) = M(0)\exp\left\{-\frac{\langle\varphi^2(t_{\text{E}})\rangle}{2}\right\}, \tag{9}$$

where

$$\langle\varphi^2(t_{\text{E}})\rangle = -2\gamma^2 \int_0^{t_{\text{E}}}\int_0^{t''} \mathrm{d}t''\,\mathrm{d}t' g(t'')q(t'')g(t') \times q(t')D(t''-t')[t''-t']. \tag{10}$$

The $D(t)$ in Eq. (10) is the time-dependent diffusion coefficient defined in Eq. (1).

For small values of $k = \gamma g\delta$, the derivative in the ideal PFGSTE expression Eq. (2) is equivalent to division by k^2. This corresponds to dividing by the exact free-space attenuation exponent [2], $g^2\gamma^2\delta^2 D_0(\Delta - \delta/3)$, in the limit of short δ. More generally, for an arbitrary pulse sequence, one can define the apparent diffusion coefficient via

$$D_{\text{app}}(t_{\text{E}}) \equiv \frac{-\ln\left(M(t_{\text{E}})/M_0\right)}{\gamma^2\int_0^{t_{\text{E}}}\int_0^{t''}\mathrm{d}t''\,\mathrm{d}t' g(t'')q(t'')g(t')q(t')(t''-t')}. \tag{11}$$

For unrestricted diffusion, the above expression gives exactly D_0. And for the PFGSTE sequence, it becomes [2,27]

$$D_{\text{app}} \equiv \frac{-\ln(M(t_{\text{E}})/M_0)}{g^2\gamma^2\delta^2(\Delta - \delta/3)}. \tag{12}$$

This procedure is well-suited to the analysis of the effects of restriction since, roughly speaking, it factors out the free attenuation.

Now we proceed to evaluate $\langle\varphi^2(t_{\text{E}})\rangle$. Let us denote the times when the RF pulses are applied, or the gradient pulses turned on and off, by $\{t_1, t_2, \ldots, t_N\}$. We define the last time marker $t_{N+1} \equiv t_{\text{E}}$ to be the echo time, and define $\tau_k \equiv t_{k+1} - t_k$ as the interval between two successive time markers. See Fig. 3 for an example of our notations. We then consider an effective gradient that is piecewise constant in time, with $g(t)q(t) = g_k q_k$ for $t \in [t_k, t_{k+1}]$. Then $\langle\varphi^2(t_{\text{E}})\rangle$ of Eq. (10) can be written as

$$\langle\varphi^2(t_{\text{E}})\rangle = \sum_{k=1}^{N}(g_k q_k)^2 K_{kk} + 2\sum_{k>l}^{N}(g_k q_k g_l q_l)K_{kl}, \tag{13}$$

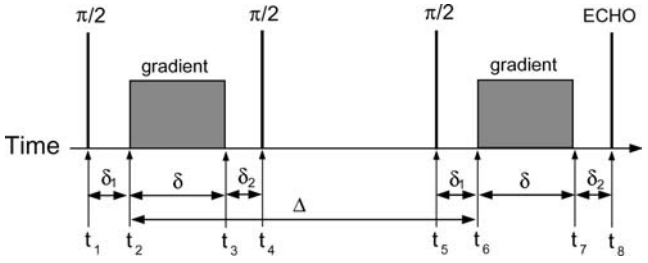

Fig. 3. Pulsed-field gradient stimulated echo (PFGSTE) pulse sequence with the notations used in this paper.

where

$$K_{kk} = 2\tau_k I_1(0,\tau_k) - 2I_2(0,\tau_k), \tag{14}$$

and for $k > l$,

$$\begin{aligned} K_{kl} = {} & I_2(t_l - t_{k+1}, t_{l+1} - t_{k+1}) \\ & - [t_l - t_{k+1}] I_1(t_l - t_{k+1}, t_{l+1} - t_{k+1}) \\ & + \tau_l I_1(t_{l+1} - t_{k+1}, t_l - t_k) + [t_{l+1} - t_k] I_1(t_l - t_k, t_{l+1} - t_k) \\ & - I_2(t_l - t_k, t_{l+1} - t_k). \end{aligned} \tag{15}$$

Here, we defined

$$\begin{aligned} I_1(t', t'') &\equiv -\gamma^2 \int_{t'}^{t''} \mathrm{d}t\, t D(t), \\ I_2(t', t'') &\equiv -\gamma^2 \int_{t'}^{t''} \mathrm{d}t\, t^2 D(t). \end{aligned} \tag{16}$$

Note that the knowledge of I_1 and I_2 completely determines the attenuation of the magnetization within the GPA.

To evaluate Eq. (16) we need a model for the time-dependent diffusion coefficient. As discussed in [21], one can use here the rigorously valid short and long-time forms of $D(t)$, Eqs. (3) and (7), respectively, to analytically compute I_1 and I_2, thus obtaining model-independent expressions for the short and long-time limits of the attenuation exponent. A general formula for $D(t)$ in an arbitrary porous medium does not exist. However, one can interpolate between Eqs. (3) and (6) using a Padé-approximant prescription [6,8]:

$$D(t) = D_0 \left[1 - \eta \frac{\sqrt{t\alpha} + t\beta}{\sqrt{t\alpha} + t\beta + \eta} \right], \tag{17}$$

where $\eta = (1 - 1/\mathcal{T})$; $\alpha = D_0[(4/9\sqrt{\pi})(S/V)]^2$ sets the time scale of validity of the short-time regime; and β determines the rate of approach to the long-time tortuosity limit. β can be related to the macroscopic homogeneity length scale of the medium, $L_{\mathrm{MACRO}} \equiv \sqrt{D_0/\beta}$, which in most physical systems will be of the order of $L_S \equiv (9\sqrt{\pi}/4)(V/S)$. In a simple pack of beads, for example, Mair et al. fits the data with $L_{\mathrm{MACRO}} \approx L_S/3$ [9]. $L_{\mathrm{MACRO}} \approx 1\,\mathrm{mm}$ corresponds to $\beta \sim 2 \times 10^{-3}\,\mathrm{s}^{-1}$ for water at room temperature and $\beta \sim 5.7\,\mathrm{s}^{-1}$ for xenon at 1 bar pressure. We note here also that the long-time expansion of the Padé form of $D(t)$ in Eq. (17) is consistent with Eq. (7) with the associations $\kappa_1 = D_0\eta^2/\beta$ and $\kappa_2 = -D_0\sqrt{\alpha}\eta^2/\beta^2$.

The Padé form of $D(t)$ in Eq. (17) is just an interpolation formula that connects the analytically derivable short- and long-time limits. Two of the parameters in it, the tortuosity $\mathcal{T}$ and the surface-to-volume ratio S/V, can be extracted from the two asymptotic regimes and, in principle, do not depend on any interpolation. The physical interpretation of the third parameter β as being related to L_{MACRO} hinges on the assumption of existence of such a single well-defined homogeneity length scale. In complex porous media, there may be many different length scales and β will in general depend on all of them. In fact, the form of Eq. (17) may not even be appropriate. However, experimentally at least, Eq. (17) seems to adequately fit most data, whether in random bead packs [8,9] or various types of porous rocks [6,30,31]. Whatever the precise interpretation of the parameter β, therefore, we expect that in most connected porous media, $D(t)$ will be well represented by the general form of Eq. (17). Using Eq. (17), the I_1 and I_2 in Eq. (16) can then be evaluated explicitly, and within the GPA should yield a good prediction of the attenuation exponent. The full expressions have been derived in [21] and we repeat them in Appendix B.

3. Application to the PFGSTE pulse sequence

We now specialize to Tanner's stimulated-echo sequence [2] which we sketch in Fig. 3. The three 90° RF pulses are applied at times t_1, $t_4 = t_1 + \tau$, and $t_5 = t_1 + \Delta$, where we let $\tau = \delta_1 + \delta + \delta_2$. The echo forms at $t_8 = t_1 + \Delta + \tau$. For simplicity, we ignore any background fields and apply an external uniform gradient $g(t) = g$ for $t_2 < t < t_3$ and $t_6 < t < t_7$ and $g(t) = 0$ otherwise. The effective gradient felt by the spins will be $q(t)g(t)$ with $q(t) = -1$ for $t_1 < t < t_4$, $q(t) = 0$ for $t_4 < t < t_5$, and $q(t) = +1$ for $t_5 < t < t_8$. The appropriate time partition is $\{\tau_1, \tau_2, \tau_3, \tau_4, \tau_5, \tau_6, \tau_7\} = \{\delta_1, \delta, \delta_2, \Delta - \tau, \delta_1, \delta, \delta_2\}$.

Now we evaluate the expressions for I_1 and I_2 from Appendix B at the appropriate times in Eqs. (14) and (15) and sum up according to Eq. (13) to obtain the attenuation exponent for the sequence. The explicit form of the general expression is rather lengthy and unilluminating, so we only write down its short- and long-time limits in subsequent sections. We used the complete general expression, however, to obtain the open-geometry curve in Fig. 2, and here we use it again to compute, via Eq. (12), the apparent diffusion coefficient D_{app} for PFGSTE. We plot it in Fig. 4 as a function of the diffusion length during Δ for three different pulse widths. The shortest length scale probed is limited by the width of the pulse δ. Curve A gives very nearly the correct $D(t)$

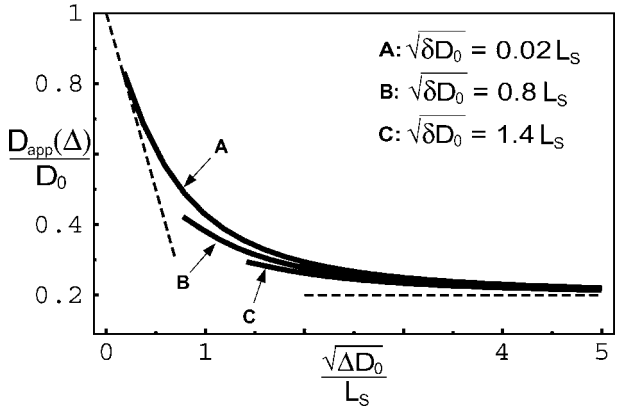

Fig. 4. The apparent diffusion coefficient, Eq. (12), in an open geometry with tortuosity $\mathcal{T} = 5$ and $\beta = \alpha$, as measured with a narrow-pulse A and finite-width pulses B and C. As before, L_S is the length scale of the open geometry defined by its surface-to-volume ratio, $L_S = (9\sqrt{\pi}/4)(V/S)$. The horizontal dashed line marks the long-time tortuosity limit, and the sloping dashed line gives the narrow-pulse short-time limit obtainable from Eq. (19) by letting $\delta \to 0$. Curves do not start at zero because, by construction, $\Delta \geqslant \delta$. Curve A overlaps completely with the narrow-pulse limit. Note that the deviations of B and C from A are quite small in the regions where $\Delta \gg \delta$.

as would be extracted from the ideal PFGSTE. Throughout most of the accessible range of Δ, the curves for pulses of finite duration, B and C, do not deviate strongly from A, and for long Δ, all three curves asymptote to the same limit as discussed in Section 3.2. Short length scales cannot be probed with finite-width pulses directly. One sometimes attempts to use Eq. (17) to fit the short-time behavior of $D(t)$ from its long-time tail [6]. Performing such a fit with curve B, for example, would overestimate the S/V by $\sim 50\%$. Our formalism, assuming the appropriateness of the Padé form of $D(t)$, yields the correct fit.

3.1. Short-Δ limit

In the short-time limit, the correction to the unbounded result is proportional to the surface-to-volume ratio (S/V) of the confining space. The computation of the attenuation exponent in this regime does not require the use of the Padé approximation. One can use the asymptotically exact short-time form of $D(t)$ in Eq. (3) to evaluate the integrals in Eq. (16) as done in [21]. Since the GPA becomes exact for short times, so does the attenuation exponent in Eq. (18). It is valid, moreover, for open and closed geometries alike. The same expression is obtained by taking the short-Δ and short-δ limit of the general Padé formula computed above using the I_1 and I_2 from Appendix B. We note lastly that, as for unbounded space, the short-time attenuation exponent depends only on δ and Δ and not on the precise positioning of the gradients between the RF pulses. We have

$$
\begin{aligned}
-\frac{\langle\varphi^2\rangle}{2}\bigg|_{\text{short}} &= -\frac{1}{3}g^2\gamma^2 D_0\Big\{\delta^2(3\Delta-\delta)+\frac{S}{V}\frac{16}{105\sqrt{\pi}} \\
&\quad\times\Big[\Delta^3\Big(2\sqrt{D_0\Delta}-\sqrt{D_0(-\delta+\Delta)} \\
&\quad-\sqrt{D_0(\delta+\Delta)}\Big)+3\delta\Delta^2\Big(\sqrt{D_0(-\delta+\Delta)} \\
&\quad-\sqrt{D_0(\delta+\Delta)}\Big)+\delta^3\Big(2\sqrt{D_0\delta} \\
&\quad+\sqrt{D_0(-\delta+\Delta)}-\sqrt{D_0(\delta+\Delta)}\Big) \\
&\quad-3\delta^2\Delta\Big(\sqrt{D_0(-\delta+\Delta)} \\
&\quad+\sqrt{D_0(\delta+\Delta)}\Big)\Big]\Big\} \qquad (18)\\
&\overset{\delta\ll\Delta}{\to} -g^2\gamma^2\delta^2 D_0\Big(\Delta-\frac{\delta}{3}\Big) \\
&\quad\times\Big[1-\frac{4}{9\sqrt{\pi}}\frac{S\sqrt{D_0\Delta}}{V}\Big(1+\frac{\delta}{3\Delta}\Big)\Big]. \qquad (19)
\end{aligned}
$$

Eq. (18) is valid provided $g^2\gamma^2\delta^2 D_0\Delta \ll 1$ and $\sqrt{D_0\Delta} \ll V/S$. Letting $\delta \ll \Delta$ gives the first-order correction to the narrow-pulse limit.

3.2. Long-Δ limit

The long-time regime is reached when the spins have diffused through a distance larger than the macroscopic length scale of the medium, $L_{\text{MACRO}} \equiv \sqrt{D_0/\beta} \approx L_S \equiv (V/S)(9\sqrt{\pi}/4)$. Here, we contrast the behavior under narrow pulses and pulses of finite duration by considering two different limiting cases.

Case 1. Narrow pulse: $\sqrt{D_0\Delta} \gg L_S$ and $\sqrt{D_0\delta} \ll L_S$,

$$
\begin{aligned}
\frac{D_{\text{app}}}{D_\infty} &\to 1+\frac{\mathcal{T}}{\Delta}\frac{\eta^2}{\beta}\Big(1-\frac{1}{3}\frac{\beta\delta}{\eta}\Big) \\
&= 1+\mathcal{T}\eta^2\frac{L^2_{\text{MACRO}}}{D_0\Delta}\Big(1-\frac{1}{3\eta}\frac{D_0\delta}{L^2_{\text{MACRO}}}\Big). \qquad (20)
\end{aligned}
$$

Case 2. Wide pulse: $\sqrt{D_0\Delta} \gg \sqrt{D_0\delta} \gg L_S$,

$$
\begin{aligned}
\frac{D_{\text{app}}}{D_\infty} &\to 1+\frac{8}{3}\frac{\mathcal{T}\eta^2}{\beta^2\Delta\delta}\frac{\sqrt{D_0\delta}}{L_S} \\
&= 1+\frac{8\mathcal{T}\eta^2}{3}\frac{L^4_{\text{MACRO}}}{D_0\Delta D_0\delta}\frac{\sqrt{D_0\delta}}{L_S}, \qquad (21)
\end{aligned}
$$

where $D_\infty = D_0/\mathcal{T}$ as defined in Eq. (6).

In either case, although the rates of approach differ, $D_{\text{app}} \to D_\infty$ reaches the same asymptotic long-Δ behavior. Thus, regardless of whether a narrow pulse or a finite-width pulse is used, D_{app} will converge to the correct value of the actual $D(t)$. Since the same was true in the short-Δ limit, D_{app} is effectively "pinned" to the correct $D(t)$ form for both short and long times. Quite generally, then, its deviation from $D(t)$ will tend to be small for all t. We examine this claim in more detail in the following Section.

Case 2 above, when both δ and Δ are long, can, in fact, be computed for the general form of the long-time

expansion of $D(t)$ in Eq. (7). As discussed in [21], one can use Eq. (7) directly in Eq. (16) to compute the first two terms in the long-time expansion of the attenuation exponent. This procedure yields a model-independent long-time formula,

$$\frac{D_{\rm app}}{D_\infty} \to 1 - \frac{8}{3}\frac{\kappa_2 \mathcal{T}}{D_0 \Delta \sqrt{\delta}}. \tag{22}$$

With the identification $\kappa_2 = -D_0\sqrt{\alpha}\eta^2/\beta^2$ as before [Eq. (17) and discussion below], Eq. (22) reduces to Eq. (21). To emphasize, Eq. (22) *does not* depend on the Padé interpolation formula in Eq. (17) but, within the GPA, is completely general.

4. Error due to the narrow-pulse approximation

In this section, we quantify the error incurred in the determination of $D(t)$ due to the breakdown of the narrow-pulse approximation. We define a percent-error parameter

$$\epsilon(\Delta,\delta) \equiv \frac{D_{\rm app}(\Delta,\delta) - D_{\rm app}(\Delta,\delta=0)}{D_{\rm app}(\Delta,\delta)} \times 100\%, \tag{23}$$

which measures the deviation of $D_{\rm app}(\Delta,\delta)$ from the narrow-pulse limit, $D_{\rm app}(\Delta,\delta=0) = D(\delta)$. Recall that when $\delta = \Delta$, the pulse has the longest possible duration, i.e., the gradient is on throughout the entire experiment. The corresponding deviation from the narrow-pulse behavior will be the strongest and thus $\epsilon(\Delta,\delta=\Delta)$ will give the "worst case" error. We plot $\epsilon(\Delta,\Delta)$ in Fig. 5 as a function of Δ for the β parameter equal to α and four different values of tortuosity, from top to bottom, $\mathcal{T}^{-1} = 0.2$, 0.3, 0.5, 0.8. For a very low tortuosity system, curve d in the figure, which could represent a suspension, the deviation due to the finite pulse width is

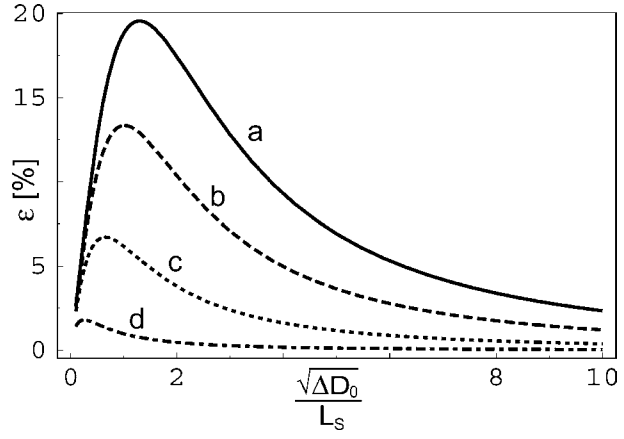

Fig. 5. The "worst case" percent error in estimated diffusion coefficient, $\epsilon(\Delta,\delta=\Delta)$, as defined in Eq. (23), plotted as a function of the diffusion length during Δ. Curves a, b, c and d correspond to $1/\mathcal{T} = 0.2$, 0.3, 0.5, and 0.8 respectively. Parameter $\beta = \alpha$ for all curves.

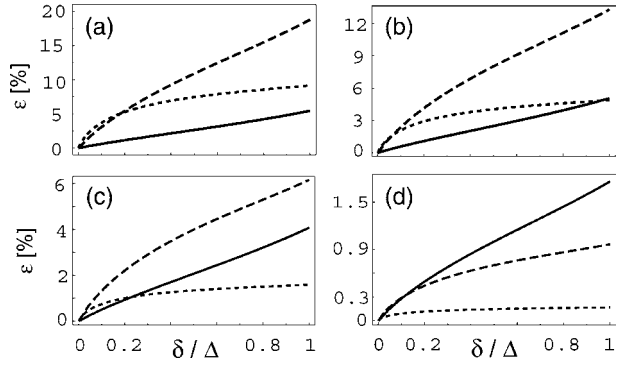

Fig. 6. The percent-error parameter ϵ, Eq. (23), as a function of δ/Δ for the four values of tortuosity $\mathcal{T}$ used in Fig. 5. Panels a, b, c and d correspond to $1/\mathcal{T} = 0.2$, 0.3, 0.5, and 0.8, respectively. In each panel, the error is shown for three different values of the diffusion length: solid line, with $\sqrt{D_0\Delta}/L_S = 0.2$, represents the short-time regime; short-dashed line, with $\sqrt{D_0\Delta}/L_S = 4$, represents the long-time regime; and long-dashed line, with $\sqrt{D_0\Delta}/L_S = 1$, belongs to the intermediate regime.

minimal, less than 2% for the entire range of Δ. For a random pack of mono-sized beads, $\mathcal{T}^{-1}$ is between 0.5 and 0.3. And for a typical reservoir rock, $\mathcal{T}^{-1}$ is on the order of 0.2. Even for these high tortuosities, the error parameter remains less than 20%. We choose a small value of β to exaggerate the difference between the long-Δ limit cases 1 and 2 in Section 3.2. For larger values of β, $D(t)$ approaches the tortuosity limit faster and the relative error for long Δ's decreases.

In Fig. 6, we plot the error parameter ϵ as a function of δ/Δ for three different values of Δ. Tortuosities used in panels a, b, c, and d correspond to the curves with the same label in Fig. 5. The solid line in all four panels corresponds to the short-time regime, with $\sqrt{D_0\Delta} = 0.2L_S$; the short-dashed line, $\sqrt{D_0\Delta} = 4L_S$, to the long-time regime; and the long-dashed line, $\sqrt{D_0\Delta} = L_S$, to the intermediate regime. As noted previously, for small tortuosities, panels c and d, the error remains small for all pulse widths and all values of Δ. We also observe that, when $\delta \ll \Delta$ the error is $\leqslant 2\%$, irrespective of tortuosity and of absolute durations of the gradient pulse δ and the diffusion time Δ.

5. Conclusions

We have investigated the effects of finite-width gradient pulses on the PFGSTE measurement of the time-dependent diffusion coefficient $D(t)$ in an open geometry, such as an extended porous medium. In the short- and long-time limits we have derived explicit model-independent formulas for the apparent diffusion coefficient $D_{\rm app}$. In these asymptotic regimes, $D_{\rm app}$ approaches the actual $D(t)$ measured using the ideal narrow-pulse PFGSTE. To study intermediate times, we assumed a well-established Padé-interpolated form of

$D(t)$ and used it to compute D_{app}. We found that, fixed by the asymptotic behavior for both short and long times, D_{app} does not deviate much from $D(t)$ for all times. More important, however, we showed that the geometric quantities of interest contained in $D(t)$, the pore surface-to-volume ratio and the tortuosity of the medium, can be extracted directly from D_{app} even when the narrow-pulse approximation breaks down and the actual $D(t)$ cannot be measured.

Acknowledgments

We are grateful to Professor Yoram Cohen of Tel-Aviv University and to Dr. Peter Basser of the National Institute of Health for urging us to work on this problem; and again to Professor Cohen for the hospitality at the Bat Shiva Conference, Tel-Aviv, 2001. Work at Harvard was partially supported by NSF Grant DMR-99-81283.

Appendix A. Gaussian phase approximation in homogeneous porous media in a uniform gradient

As indicated in Fig. 7, the GPA in a porous medium will be valid in three different regimes: First, when the phases accumulated by the spins throughout the entire experiment are small (lower left-hand corner in the Figure); second, when both Δ and δ are long, regardless of the phase acquired (upper right-hand corner); and third, when Δ is long and the phases accumulated during just the encoding (or decoding) period are small (lower right-hand corner). In fact, these three regimes will merge for a sufficiently weak gradient (long t^* in the figure), making the GPA valid for all Δ and δ. We now discuss each regime in turn.

When the distribution of spin phases at echo time is narrowly peaked around $\langle\varphi\rangle = 0$, i.e. the spins have acquired only very little phase, the GPA will be a good approximation simply because the higher moments are much smaller than the variance, $1 \gg \langle\varphi^2\rangle \gg \langle\varphi^3\rangle \gg \cdots$ This situation will occur for sufficiently short times (both δ and Δ), regardless of gradient strength, but also for any Δ and δ given sufficiently weak gradient. Both cases can be rigorously treated via a direct perturbative expansion of the Torrey–Bloch equation in the field inhomogeneity, in a Dyson-like series, as done for instance in [21,25]. This regime is not limited just to porous media, but will obtain in arbitrary geometries, whether open or closed. We indicate it in Fig. 7 by the shaded region in the lower-left corner, with t^* fixed by the strength of the gradient, as defined in the caption.

To discuss the other two regimes, we specialize to a homogeneous porous medium, characterized by a macroscopic homogeneity length scale L_{MACRO} and the typical time to traverse it t_M. Following the usual approach [4,32], we consider a random walker taking a step every time interval τ and in the ith step moving parallel to the gradient g from x_i to $x_{i+1} = x_i + \delta x_i$. (We can ignore motion in the plane transverse to the direction of the gradient.) δx_i are drawn from a symmetric distribution of step sizes $P(\delta x)$, with zero mean and a finite second moment σ. $P(\delta x)$ reflects the fact that spins near the walls take shorter steps in time τ than the spins in the bulk; in our framework, $P(\delta x)$ is the only way through which restriction bears on the motion of the molecules. This picture will be valid provided that any region of size L_{MACRO} has, as far as diffusion is concerned, the same statistical properties. This is what we mean by a *homogeneous* porous medium. More specifically, we make the following three assumptions about the system under consideration:

1. $\langle\delta x_i \delta x_{i+N}\rangle = 0$ for $N\tau > t_M$, i.e., the steps taken by a spin become uncorrelated after it has traversed L_{MACRO}.
2. For $N\tau > t_M$, the distribution of the spin's total displacement, $\sum_{i=1}^{N} \delta x_i$, becomes independent of where it started and approaches a Gaussian with an effective diffusion coefficient D_∞.

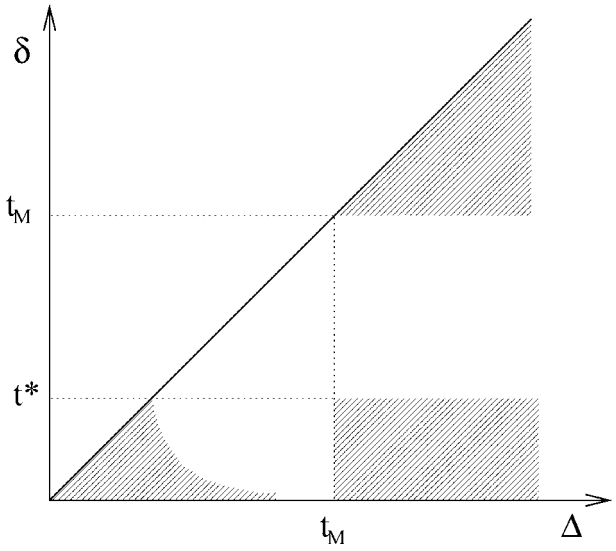

Fig. 7. Thatched regions mark the regimes of validity of the GPA in a connected porous medium for the PFGSTE with δ and Δ as labeled in Fig. 3. By definition $\delta < \Delta$, and thus the accessible phase space is restricted to the lower triangle. t_M is the time to diffuse across the inhomogeneity length scale of the medium; and t^*, defined via $\gamma g t^* (D_0 t^*)^{1/2} = \pi$, marks the time scale at which the phase acquired while the pulse is on becomes significant. The curved line, given by $\gamma g \delta (D_0 \Delta)^{1/2} = \pi$, bounds the small-$\varphi$ regime (lower left-hand corner), where the GPA holds since the higher moments of the phase distribution are much smaller than the variance. As discussed in the text, the GPA will also hold when both $\delta, \Delta > t_M$ (upper right-hand corner) and when $\Delta > t_M$ and $\delta < t^*$ (lower right-hand corner). Note that for a sufficiently weak gradient, t^* may be in fact longer than t_M, shading in the entire lower triangle and making the GPA valid for all times.

3. The gradient is sufficiently weak so that the spins do not dephase much during t_M; if the gradient is strong, we enter the "localization regime," and the GPA breaks down [24,34,33].

The first two conditions characterize the medium (irrespective of the magnetic field), and the third one pertains to the interaction of the spins with the applied gradient.

We consider the PFGSTE from Fig. 3, with $\delta = n\tau$ and $\Delta = (p+n)\tau$. The phase acquired by a spin along its trajectory is given by

$$\begin{aligned}\varphi &= \gamma g\tau \sum_{j=1}^{n} x_j - \gamma g\tau \sum_{k=1}^{n} x_{n+p+k} \\ &= \gamma g\tau \sum_{j=1}^{n} (x_j - x_{n+1}) - \gamma g\tau \sum_{k=1}^{n} (x_{n+p+k} - x_{n+p}) \\ &\quad - \gamma g\tau n (x_{n+p} - x_{n+1}) \\ &= \underbrace{-\gamma g\tau \sum_{j=1}^{n} j\delta x_j}_{\varphi_{\mathrm{enc}}} \underbrace{- \gamma g\tau \sum_{j=0}^{n-1} (n-j)\delta x_{n+p+j}}_{\varphi_{\mathrm{dec}}} \underbrace{- \gamma g\tau n \sum_{j=1}^{p-1} \delta x_{n+j}}_{\varphi_{\mathrm{store}}}.\end{aligned} \tag{A.1}$$

Here φ_{enc} and φ_{dec} are the phases acquired during the encoding and decoding periods, respectively, and φ_{store} is due to translation during the storage period. For free diffusion, φ_{enc}, φ_{dec}, and φ_{store} are uncorrelated, and each independently has a Gaussian distribution with zero mean. Consequently, the distribution of φ will be Gaussian as well.

When $p\tau \gg t_M$, i.e., Δ is long, by our assumptions about the homogeneous porous medium, again φ_{enc}, φ_{dec}, and φ_{store} become uncorrelated. The distribution of φ_{store} will still be Gaussian, but distributions of φ_{enc} and φ_{dec} in general need not be, and neither does the distribution of φ. If, however, $n\tau \gg t_M$, i.e., δ is long as well, then conditions (1) and (2) above imply that each spin during δ will have mapped out the entire step-size distribution $P(\delta x)$. We can then reshuffle all the terms in the expressions for φ_{enc} and φ_{dec} in Eq. (A.1), effectively making all the δx_j into independent identically distributed variables. Following [32], one can then show that the Central Limit Theorem will apply to each sum, proving that the distributions of φ_{enc} and φ_{dec} will each tend to a Gaussian, and thus so will the distribution of φ.

Finally, when $\Delta > t_M$ and φ_{enc} and φ_{dec} are small because $\gamma g\delta (D_0\delta)^{1/2} \ll 1$, again the distributions of φ_{store}, φ_{enc} and φ_{dec} will be each approximately Gaussian with zero mean. Thus, the distribution of φ will be near-Gaussian as well. As is apparent from Eq. (2), in the measurement of diffusivities, one is primarily interested in the limit of small $k = \gamma g\delta$; this is true even when the narrow-pulse approximation is inapplicable. The GPA in this case will be valid for short Δ and for long Δ and will provide an interpolating formula in the intermediate range. In fact, if the gradient is sufficiently weak so that $\gamma g\delta (D_0\Delta)^{1/2} \ll 1$, then the GPA will be a good approximation for the whole range of Δ and δ. A phase diagram of all three regimes is sketched in Fig. 7.

Appendix B. Explicit formulas for I_1 and I_2 in Eq. (16)

Performing the integrals in Eq. (16) for the Padé model of $D(t)$ in Eq. (17), one obtains

$$\begin{aligned}\frac{I_1(t',t'')}{\gamma^2} &= \frac{t^2(-1+\eta)}{2} + \frac{2\sqrt{t\alpha}\eta^2}{\beta^2} - \frac{t\eta^2}{\beta} \\ &\quad + \left\{ 2\sqrt{\alpha}\eta^2(\alpha - 3\beta\eta) \arctan\left((\sqrt{\alpha} + 2\sqrt{t\beta}) \Big/ \left(\sqrt{4\beta\eta - \alpha}\right)\right)\right\} \Big/ \left\{ \sqrt{4\beta\eta - \alpha}\beta^3 \right\} \\ &\quad + \left. \frac{\eta^2(-\alpha + \beta\eta)\log(\sqrt{t\alpha} + t\beta + \eta)}{\beta^3} \right|_{t'}^{t''}, \\ \frac{I_2(t',t'')}{\gamma^2} &= \frac{t^3(-1+\eta)}{3} + \frac{2t^{\frac{3}{2}}\sqrt{\alpha}\eta^2}{3\beta^2} - \frac{t^2\eta^2}{2\beta} \\ &\quad + \frac{2\sqrt{t\alpha}\eta^2(\alpha - 2\beta\eta)}{\beta^4} + \frac{t\eta^2(-\alpha + \beta\eta)}{\beta^3} \\ &\quad + \left\{ 2\sqrt{\alpha}\eta^2(\alpha^2 - 5\alpha\beta\eta + 5\beta^2\eta^2) \right. \\ &\quad \left. \times \arctan\left((\sqrt{\alpha} + 2\sqrt{t\beta}) \Big/ \left(\sqrt{4\beta\eta - \alpha}\right)\right)\right\} \\ &\quad \Big/ \left\{ \sqrt{4\beta\eta - \alpha}\beta^5 \right\} \\ &\quad - \left. \frac{\eta^2(\alpha^2 - 3\alpha\beta\eta + \beta^2\eta^2)\log(\sqrt{t\alpha} + t\beta + \eta)}{\beta^5} \right|_{t'}^{t''},\end{aligned} \tag{B.1}$$

where the antiderivative in t is to be evaluated at the endpoints t' and t'' according to the appropriate time partition in Eqs. (13)–(15).

References

[1] E.O. Stejskal, J.E. Tanner, Spin diffusion measurements: spin echoes in the presence of a time-dependent field gradient, J. Chem. Phys. 42 (1965) 288.
[2] J.E. Tanner, Use of the stimulated echo in NMR diffusion studies, J. Chem. Phys. 52 (5) (1970) 2523.
[3] J. Kärger, H. Pfeifer, W. Heink, Principles and application of self-diffusion measurements by nuclear magnetic resonance, in: J.S. Waugh (Ed.), Advances in Magnetic Resonance, vol. 12, Academic Press, 1988, pp. 1–89.
[4] P.T. Callaghan, Principles of Nuclear Magnetic Resonance Microscopy, Oxford University Press, New York, 1993.
[5] P.P. Mitra, P.N. Sen, L.M. Schwartz, Short-time behavior of the diffusion coefficient as a geometrical probe of porous media, Phys. Rev. B 47 (1993) 8565.
[6] M.D. Hürlimann, K.G. Helmer, L.L. Latour, C.H. Sotak, Restricted diffusion in sedimentary rocks. Determination of

surface-area-to-volume ratio and surface relaxivity, J. Magn. Reson. Ser. A 111 (1994) 169–178.
[7] P.N. Sen, L.M. Schwartz, P.P. Mitra, B.I. Halperin, Surface relaxation and the long-time diffusion coefficient in porous media: periodic geometries, Phys. Rev. B 49 (1994) 215.
[8] L. Latour, P. Mitra, R. Kleinberg, C. Sotak, Time-dependent diffusion coefficient of fluids in porous media as a probe of surface-to-volume ratio, J. Magn. Reson. Ser. A 101 (1993) 342–346.
[9] R.W. Mair, P.N. Sen, M.D. Hürlimann, S. Patz, D.G. Cory, R.L. Walsworth, Narrow pulse approximation and long length scale determination in xenon gas diffusion NMR studies of model porous media, J. Magn. Reson. 156 (2002) 202.
[10] L.Z. Wang, A. Caprihan, E. Fukushima, The narrow-pulse criterion for pulsed-gradient spin-echo diffusion measurements, J. Magn. Reson. Ser. A 117 (1995) 209–219.
[11] A. Caprihan, L.Z. Wang, E. Fukushima, A multiple-narrow-pulse approximation for restricted diffusion in a time-varying field gradient, J. Magn. Reson. Ser. A 118 (1996) 94–102.
[12] M.H. Blees, The effect of finite duration of gradient pulses on the pulsed-field-gradient NMR method for studying restricted diffusion, J. Magn. Reson. Ser. A 109 (1994) 203.
[13] P. Linse, O. Söderman, The validity of the short-gradient-pulse approximation in NMR studies of restricted diffusion. Simulations of molecules diffusing between planes, in cylinders and spheres, J. Magn. Reson. Ser. A 116 (1995) 77–86.
[14] P.P. Mitra, B.I. Halperin, Effects of finite gradient-pulse widths in pulsed-field-gradient diffusion measurements, J. Magn. Reson. Ser. A 113 (1995) 94.
[15] Y. Cohen, Y. Assaf, R. Mossin-Manor, I.E. Biton, Diffusion and q-space diffusion MRI in cerebral ischemia to multiple sclerosis and beyond, in: Blood Brain Barrier Delivery and Brain Pathology, NATO ASI Series, Kluwer Academic Publishers, submitted.
[16] R.L. Kleinberg, Well logging, in: Encyclopedia of Nuclear Magnetic Resonance, vol. 8, Wiley, Chichester, 1996, pp. 4960–4969.
[17] J.R.F. Karlicek, I.J. Lowe, A modified pulsed gradient technique for measuring diffusion in the presence of large background gradients, J. Magn. Reson. 37 (1980) 75.
[18] J.S. Murday, R.M. Cotts, Self-diffusion coefficient of liquid lithium, J. Chem. Phys. 48 (1968) 4938.
[19] G.H. Sørland, B. Hafskjold, O. Herstad, A stimulated-echo method for diffusion measurement in heterogeneous media using pulsed field gradients, J. Mag. Reson. 124 (1997) 172–176.
[20] J.G. Seland, G.H. Sørland, K. Zick, B. Hafskjold, Diffusion measurements at long observation times in the presence of spatially variable internal magnetic field gradients, J. Mag. Reson. 146 (2000) 14–19.
[21] L.J. Zielinski, P.N. Sen, Combined effects of diffusion, non-uniform-gradient magnetic fields, and restriction on an arbitrary coherence pathway, J. Chem. Phys., accepted for publication.
[22] C.H. Neuman, Spin echo of spins diffusing in a bounded medium, J. Chem. Phys. 60 (1974) 4508.
[23] B. Balinov, B. Jønsson, P. Linse, O. Söderman, The NMR self-diffusion method applied to restricted diffusion. Simulation of echo attenuation from molecules in spheres and between planes, J. Magn. Reson. Ser. A 104 (1993) 17.
[24] L.J. Zielinski, P.N. Sen, Relaxation of nuclear magnetization in a nonuniform magnetic field gradient and in restricted geometry, J. Magn. Reson. 147 (2000) 95–103.
[25] S. Axelrod, P.N. Sen, Nuclear magnetic resonance spin echoes for restricted diffusion in an inhomogeneous field: methods and asymptotic regimes, J. Chem. Phys. 114 (2001) 6878.
[26] T.M. de Swiet, P.N. Sen, Time dependent diffusion coefficient in a disordered medium, J. Chem. Phys. 104 (1996) 206.
[27] J.E. Tanner, Transient diffusion in a system partitioned by permeable barriers. Application to NMR measurements with a pulsed field gradient, J. Chem. Phys 69 (4) (1978) 1748–1754.
[28] R.R. Ernst, G. Bodenhausen, A. Wokaun, Principles of Nuclear Magnetic Resonance in One and Two Dimensions, Oxford University Press, New York, 1994.
[29] M.D. Hürlimann, Diffusion and relaxation effects in general stray field NMR experiments, J. Magn. Reson. 148 (2001) 367–378.
[30] M.D. Hürlimann, L.L. Latour, C.H. Sotak, Diffusion measurements in sandstone core: NMR determination of surface-to-volume ratio and surface relaxivity, Magn. Reson. Imag. 12 (1994) 325–327.
[31] Y.-Q. Song, Determining pore sizes using an internal magnetic field, J. Mag. Reson. 143 (2000) 397–401.
[32] H.Y. Carr, E.M. Purcell, Effects of diffusion on free precession in NMR experiments, Phys. Rev. 94 (1954) 630.
[33] T.M. de Swiet, P.N. Sen, Decay of nuclear magnetization by bounded diffusion in a constant field gradient, J. Chem. Phys. 100 (1994) 5597.
[34] M.D. Hürlimann, K.G. Helmer, T.M. de Swiet, P.N. Sen, C.H. Sotak, Spin echoes in a constant gradient and in the presence of simple restriction, J. Magn. Reson. Ser. A 113 (1995) 260–264.